Two-Dimensional Intraventricular Flow Mapping by Digital Processing Conventional Color-Doppler Echocardiography Images

Damien Garcia, Juan C. del Álamo, David Tanné, Raquel Yotti, Cristina Cortina, Éric Bertrand, José Carlos Antoranz, Esther Pérez-David, Régis Rieu, Francisco Fernández-Avilés, and Javier Bermejo*

***Abstract*—Doppler echocardiography remains the most extended clinical modality for the evaluation of left ventricular (LV) function. Current Doppler ultrasound methods, however, are limited to the representation of a single flow velocity component. We thus developed a novel technique to construct 2D time-resolved (2D+t) LV velocity fields from conventional transthoracic clinical acquisitions. Combining color-Doppler velocities with LV wall positions, the cross-beam blood velocities were calculated using the continuity equation under a planar flow assumption. To validate the algorithm, 2D Doppler flow mapping and laser particle image velocimetry (PIV) measurements were carried out in an atrio-ventricular duplicator. Phase-contrast magnetic resonance (MR) acquisitions were used to measure *in vivo* the error due to the 2D flow assumption and to potential scan-plane misalignment. Finally, the applicability of the Doppler technique was tested in the clinical setting. *In vitro* experiments demonstrated that the new method yields an accurate quantitative description of the main vortex that forms during the cardiac cycle (mean error $< 25\%$ for vortex radius, position and circulation). MR image analysis evidenced that the error due to the planar flow assumption is close to 15% and does not preclude the characterization of major vortex properties neither in the normal nor in the dilated LV. These results are yet to be confirmed by a head-to-head clinical validation study. Clinical Doppler studies showed that the method is readily applicable and that a single large anterograde vortex develops in the healthy ventricle while supplementary retrograde swirling structures may appear in the diseased heart. The proposed echocardiographic method based on the continuity equation is fast, clinically-compliant and does not require complex training. This technique will potentially enable investigators to study of additional quantitative aspects of intraventricular flow dynamics in the clinical setting by high-throughput processing conventional color-Doppler images.**

***Index Terms*—Cardiovascular system, color-Doppler, echocardiography, fluid flow, image processing.**

Manuscript received February 06, 2010; revised April 23, 2010; accepted April 27, 2010. Date of publication June 17, 2010; date of current version September 24, 2010. This work was supported in part by the Natural Sciences and Engineering Research Council of Canada under Grant BP306188 (DG), in part by the Ministerio de Ciencia e Innovación (Spain), in part by the U.S. Department of State (Fubright Program, JCdA), in part by the Fundación de Investigación Médica Mutua Madrileña of Spain, in part by the Canadian Institutes of Health Research under Grant MOP 67123 (RR), and in part by the Ministerio de Ciencia e Innovación-Instituto de Salud Carlos III (Spain) under Grants PI061101, Grant PI071100, Grant CM06/00085 (CC), and Grant RD06/0014 RECAVA. *Asterisk indicates corresponding author.*

D. Garcia is with the CRCHUM-Research Centre, University of Montreal Hospital, Montreal, QC H2L 2W5, Canada.

J. C. del Álamo is with the Department of Mechanical and Aerospace Engineering, University of California San Diego, La Jolla, CA 92093 USA.

D. Tanné, É. Bertrand, and R. Rieu are with the Biomechanics Cardiovascular Team, IRPHE, UMR 6594, CNRS, Aix-Marseille Université, 13013 Marseille, France.

R. Yotti, C. Cortina, E. Pérez-David, and F. Fernández-Avilés are with the Department of Cardiology, Hospital General Universitario Gregorio Marañón, 28007 Madrid, Spain.

J. C. Antoranz is with the Department of Mathematical Physics and Fluids, Universidad Nacional de Educación a Distancia, 28040 Madrid, Spain.

*J. Bermejo is with the Department of Cardiology, Hospital General Universitario Gregorio Marañón, 28007 Madrid, Spain (e-mail: javbermejo@jet.es).

Color versions of one or more of the figures in this paper are available online at http://ieeexplore.ieee.org.

Digital Object Identifier 10.1109/TMI.2010.2049656

I. Introduction

BECAUSE it is fully noninvasive, portable and inexpensive, Doppler-echocardiography is the most generalized imaging technique used for cardiovascular diagnosis. The combination of the cross-sectional, spectral and color-Doppler echocardiography modalities has been extensively validated in most cardiovascular diseases [1] in terms of therapeutic, patient-outcome, and societal efficacies [2]. Additional to online-assessment, a number of algorithms have proved the clinical value of digital postprocessing color-Doppler echocardiographic images. Nowadays, it is possible to obtain accurate measurements of cardiac output and regurgitant volumes using these methods. Furthermore, it has been demonstrated that left ventricular (LV) systolic and diastolic chamber function can be characterized by deriving intracardiac pressure gradients from color-Doppler M-mode echocardiograms, provided that the flow streamlines can be coaxially interrogated with the ultrasound beam [3]–[6].

Two-dimensional color-Doppler imaging is based on measuring the phase difference between transmitted and received echoes for each sample volume in the ultrasound sector [7]. This method is accurate but it only provides the flow velocity projection parallel to the direction of the ultrasound beam. Such a 1D approach constitutes a particular limitation of echocardiography given the 3D nature of intracardiac flows.

Studies using either numerical simulation [8]–[12] or *in vitro* experiments [13]–[16] have suggested that potentially relevant information can be derived from the full spatial characterization of intraventricular fluid dynamics. Special attention has been paid to swirling asymmetries of the diastolic blood flow inside the LV chamber, which have been proposed to minimize the dissipation of kinetic energy, therefore optimizing myocardial efficiency [10], [17]. These findings may have important potential medical relevance since cardiomyopathies alter the organization of LV filling flow [17], [18].

Phase-contrast magnetic resonance (MR) studies have confirmed the swirling nature of flow in the LV [19], [20]. However phase-contrast MR, is expensive, time consuming, and limited to a low temporal resolution [21], [22]. Hence, a full-flow mapping derived from echocardiography data would undoubtedly play a major role in the clinical setting. The objective of the present study was to design a novel echocardiographic method to determine intracardiac velocity vectors for routine clinical applications.

Based on the continuity equation, we developed an original algorithm to visualize the time evolution of the 2D flow field inside the LV. To validate the method, simultaneous color-Doppler and laser particle image velocimetry (PIV, [23]) measurements were obtained in an atrio-ventricular duplicator under variable hemodynamic conditions. The potential error of the method related to the planar flow assumption and to scan plane missalingnment was tested *in vivo* in a small set of phase-contrast MR studies obtained from normal and dilated ventricles. And finally, conventional echocardiographic acquisitions were performed in healthy volunteers and patients to demonstrate the applicability and accuracy of the technique in the clinical setting. Special attention was given to characterize the dynamics of the filling vortex rings.

II. Materials and Methods

Blood flow in the LV is unsteady, 3D and shows a range of different length scales [17], [24]. We focused on eddies of sizes comparable to that of the ventricular cavity. These eddies are governed by the time-varying mitral inflow and geometry of the LV, and therefore are reproducible from beat to beat in the absence of rhythm disorders. They are also most relevant to the study of ventricular function, as they carry most of the blood volume in the LV because of their large size.

In this work we focused on the large flow structures in apical long-axis plane of the LV, passing through the LV apex, the center of the mitral and of the aortic valves in the apical long-axis view. Although intracardiac flow in this location is known to be 3D, phase-contrast MR studies have shown that clinically useful parameters of intraventricular flow dynamics can be obtained from a planar flow simplification using this long-axis view. In particular, Thompson and McVeigh [25] in a small group of subjects showed that accurate pressure differences can be calculated using 2D acquisitions because the momentum fluxes normal to the plane of interest are negligible. We hypothesized that the error related to the planar flow assumption is small enough not to preclude obtaining clinically useful parameters of intraventricular flow dynamics. Specific *in vitro* (pulse-duplicator) and *in vivo* (phase-contrast MR) experiments were designed to test the error related to this planar flow assumption (see Sections II-GII–I).

A. Computation of the 2D Velocity Mapping

Assuming a 2D flow at the long-axis plane, the flux of mass normal to this plane can be neglected in the mass conservation equation, enabling us to reconstruct the second component of the blood velocity from echocardiographic color Doppler images. Adopting a polar coordinate system centered at the head of the cone-beam ultrasound probe (Fig. 1), the Doppler signal provides the radial component of the blood velocity (V_r). Although azimuthal velocities (V_θ) cannot be measured by Doppler since they are perpendicular to the ultrasound beams, they can be recovered at any specific instant of the cardiac cycle using the 2D continuity equation in polar coordinates

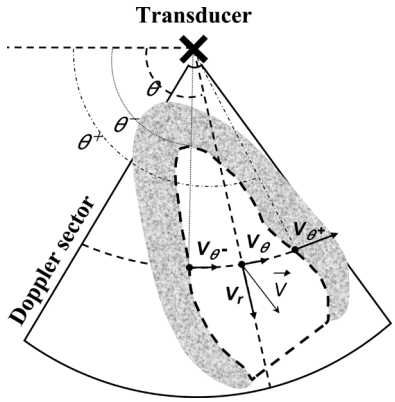

Fig. 1. Sketch of an echocardiographic acquisition in the apical long-axis view. The dashed outline delimits the plane of interest corresponding to the LV cavity. $\vec{V}$ represents the velocity of a given blood particle, V_r is its radial component measured by color-Doppler, and V_θ the azimuthal component to be determined using the continuity equation. $V_{\theta-}$ and $V_{\theta+}$ are the azimuthal velocities at the posterior and anteroseptum walls [(2)], respectively.

$$\partial_\theta V_\theta(r,\theta) = -r\partial_r V_r(r,\theta) - V_r(r,\theta). \tag{1}$$

This equation relates the azimuthal (V_θ) and radial Doppler (V_r) velocities through a simple, first-order partial differential equation that can be solved once a boundary condition is provided. Equation (1) is solved within the area delimited by the inner ventricular wall. The time-varying position of the boundaries (see Section II-C and Fig. 2) can be obtained from the B-mode layer using a number of processing techniques. For clinical studies, we used a commercially available speckle-tracking algorithm (EchoPAC, General Electric Healthcare, Horten, Norway, version 6.0.0) [26]. For *in vitro* and MR studies, the endocardial boundary was manually segmented. The tracking algorithm allows us to determine the azimuthal velocities at the posterior and anteroseptal walls of the LV. These velocities are denoted $V_\theta - (r)$ and $V_\theta + (r)$, respectively, where $\theta^-(r)$ and $\theta^+(r)$ are the azimuthal coordinates of the posterior and anteroseptal LV walls, respectively (Fig. 1). The availability of two boundary conditions makes any linear combination of the two following expressions a solution to (1)

$$V_\theta^-(r,\theta) = V_{\theta-}(r) + \int_{\theta-}^{\theta} \partial_\vartheta V_\vartheta(r,\vartheta)\mathrm{d}\vartheta$$
$$V_\theta^+(r,\theta) = V_{\theta+}(r) - \int_{\theta}^{\theta+} \partial_\vartheta V_\vartheta(r,\vartheta)\mathrm{d}\vartheta. \tag{2}$$

This extra information can be used to reduce the error in the calculation of the azimuthal velocity by combining $V_\theta^-(r,\theta)$

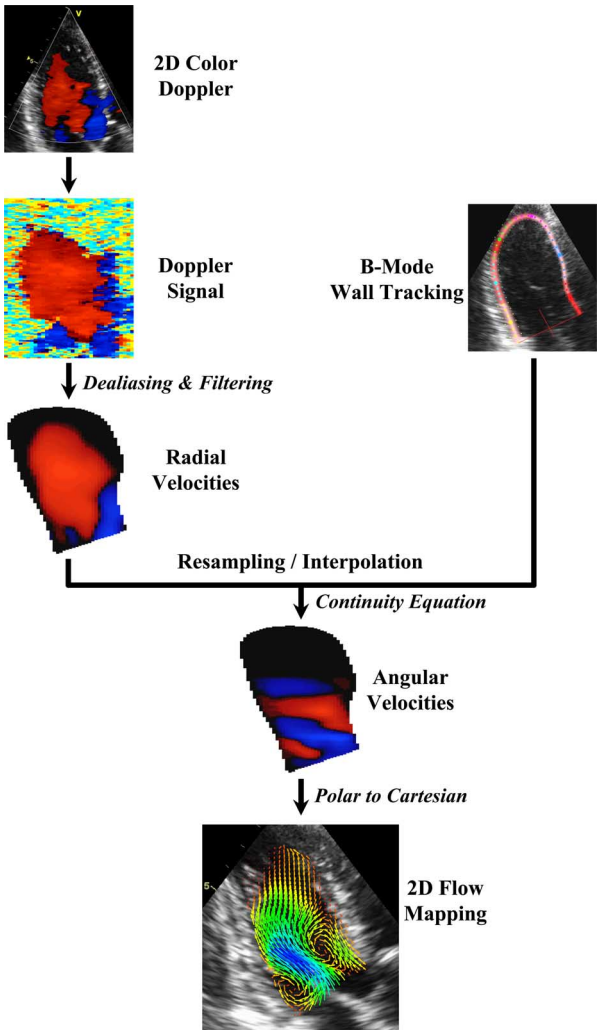

Fig. 2. Flowchart of the method of Doppler and B-mode acquisitions and digital image processing for the reconstruction of the azimuthal velocity component.

and $V_\theta^+(r,\theta)$ with a weight function $w(r,\theta)$, i.e., $V_\theta = wV_\theta^- + (1-w)V_\theta^+$, which yields

$$V_\theta = \lfloor wV_{\theta^-} + (1-w)V_{\theta^+} \rfloor + \left[w \int_{\theta^-}^{\theta} \partial_\vartheta V_\vartheta \mathrm{d}\vartheta - (1-w) \int_{\theta}^{\theta^+} \partial_\vartheta V_\vartheta \mathrm{d}\vartheta \right]. \quad (3)$$

Ideally, the azimuthal velocity should be independent of the choice of $w(r,\theta)$. The errors associated to the planar flow assumption are minimized when the weight function is chosen such that the contributions of the two solutions in (2) to V_θ are uniformly equal. Notice that this is not equivalent to $w = 0.5$, which sets uniformly equal weights for the two solutions (2) but not uniform contributions. Instead, one has

$$w(r,\theta) = 1 - \frac{\int_{\theta^-}^{\theta} [\partial_\vartheta V_\vartheta(r,\vartheta) - \partial_\vartheta V_\vartheta(r,\theta^-)]\,\mathrm{d}\vartheta}{\int_{\theta^-}^{\theta^+} [\partial_\vartheta V_\vartheta(r,\vartheta) - \partial_\vartheta V_\vartheta(r,\theta^-)]\,\mathrm{d}\vartheta} = \frac{\int_{\theta}^{\theta^+} [\partial_\vartheta V_\vartheta(r,\vartheta) - \partial_\vartheta V_\vartheta(r,\theta^+)]\,\mathrm{d}\vartheta}{\int_{\theta^-}^{\theta^+} [\partial_\vartheta V_\vartheta(r,\vartheta) - \partial_\vartheta V_\vartheta(r,\theta^+)]\,\mathrm{d}\vartheta}. \quad (4)$$

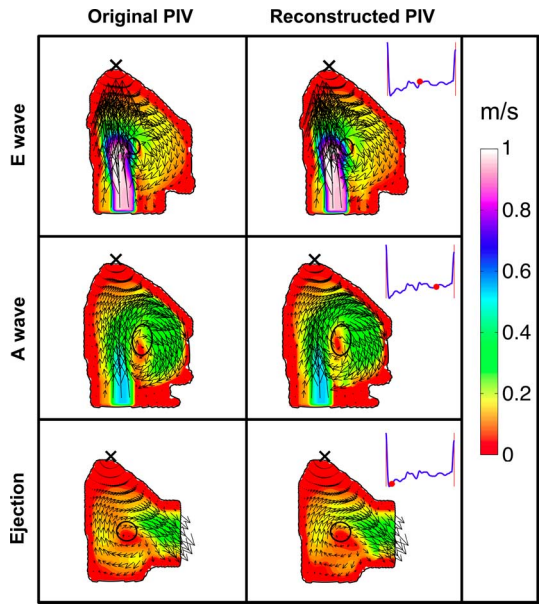

Fig. 3. Two-dimensional velocity field (m/s) in the *in vitro* model at 60 bpm, showing original PIV measurements (V_{rPIV} and $V_{\theta\mathrm{PIV}}$, left column) versus velocity field reconstructed from the continuity equation (V_{rPIV}, $V_{\theta\mathrm{REC}}$, right column). Each row shows a different time instant during the cardiac cycle. The black cross represents the virtual transducer head whereas the black circles indicate the location and radius of the main swirling region. Both color and arrow-length encode velocity magnitude.

The above expression causes problems for some values of r when the integral in the denominator becomes very small, which can be removed by choosing the weight function

$$w(r,\theta) = 1 - \frac{\int_{\theta^-}^{\theta} [\partial_\vartheta V_\vartheta(r,\vartheta) - \min(\partial_\vartheta V_\vartheta)(r)]\,\mathrm{d}\vartheta}{\int_{\theta^-}^{\theta^+} [\partial_\vartheta V_\vartheta(r,\vartheta) - \min(\partial_\vartheta V_\vartheta)(r)]\,\mathrm{d}\vartheta} = \frac{\int_{\theta}^{\theta^+} [\partial_\vartheta V_\vartheta(r,\vartheta) - \min(\partial_\vartheta V_\vartheta)(r)]\,\mathrm{d}\vartheta}{\int_{\theta^-}^{\theta^+} [\partial_\vartheta V_\vartheta(r,\vartheta) - \min(\partial_\vartheta V_\vartheta)(r)]\,\mathrm{d}\vartheta} \quad (5)$$

where $\partial_\varphi V_\varphi$ is given by (1). This weight function decreases monotonically from 1 to 0 from one wall to the other. The findings from the *in vitro* validation indicated that the results obtained using the weight function in (5) differed little from the results obtained with the optimal weight function (4) when the latter is numerically well-defined. The azimuthal velocity at the ventricular walls is obtained by imposing the free-slip impermeability boundary condition. This condition is preferred to the proper no-slip one because the spatial resolution of the color-Doppler is not fine enough to capture the thin boundary layers that form near the LV inner wall. If we denote (t_r, t_θ) the polar coordinates of a unit vector tangent to the wall, we thus obtain

$$V_{\theta^-} = V_r(\theta^-)t_\theta(\theta^-)/t_r(\theta^-)$$

and

$$V_{\theta^+} = V_r(\theta^+)t_\theta(\theta^+)/t_r(\theta^+) \quad (6)$$

where $V_r(\theta^-)$ and $V_r(\theta^+)$ are the radial velocities at the wall surface given by Doppler echocardiography. In the *in vitro* experiments, the limits of the color-Doppler acquisition sector, $\theta^-(r)$ and $\theta^+(r)$, did not coincide with the ventricular wall but with the outflow tract (see Fig. 3). Therefore, the impermeability conditions (6) were not correct when the aortic valve was open.

These conditions were replaced by imposing the direction of the velocity along the permeable boundary. This direction was set parallel to the wall of the outflow tract at each one of the two points where the former intersects with the LV walls, and letting it vary linearly along the permeable boundary from the first point to the second. Notice that this option is uniformly compatible with the impermeability condition at the LV walls (6). Several other approaches, such as least-square fitting the direction of the outflow jet, were tested and discarded. The 2D velocity field of the cardiac blood (V_r, V_θ) can finally be obtained by means of (3), (5), and (6).

B. Vortex Identification and Characterization

Vortices were identified in the reconstructed 2D velocity fields using the second invariant of the velocity gradient tensor, Q [27] (dimension$= 1/\text{time}^2$). A point (x, y) is considered to belong to a vortex of interest (VOI) if $Q(x, y) > Q_{\text{th}}$ where Q_{th} is a positive threshold that is typically chosen as $0.1 \times \max_{\text{VOI}}(Q)$. For each frame, sets of connected points belonging to a vortex were clustered into blobs which were labeled using standard image processing techniques included in Matlab (The Mathworks, Nattick, MA). Small, spurious vortex blobs were removed automatically by thresholding their area. The vortices were characterized in terms of the zeroth-, first-, and second-order moments of their vorticity distribution $\omega(x, y)$, which yielded their circulation, the trajectory of their center, and their radius and eccentricity, respectively. The circulation inside the vortex was defined as

$$\Gamma = \int_{\Omega} \omega(x, y) \mathrm{d}\Omega \tag{7}$$

where the 2D domain of integration Ω was the inner core of the vortex as defined by the Q-threshold, and $(x_{\text{v}}, y_{\text{v}})$ is the position of the vortex center given by

$$\begin{pmatrix} x_v \\ y_v \end{pmatrix} = \frac{\int_\Omega \omega(x, y) \binom{x}{y} \mathrm{d}\Omega}{\Gamma}. \tag{8}$$

The radius of the vortex was defined by

$$R = \sqrt{\frac{\int_\Omega \omega(x, y) \left((x - x_v)^2 + (y - y_v)^2\right) \mathrm{d}\Omega}{\Gamma}}. \tag{9}$$

The vortex properties were obtained independently of the Q-threshold by letting Ω be the inner domain of the circle defined by R and iterating.

C. Echocardiographic Acquisitions

Echocardiographic images of the LV were acquired in the long-axis view from the apical position (Fig. 1) using either a Vivid i (GE Healthcare) or a Vivid 7 ultrasound machine for *in vitro* and *in vivo* recordings, respectively, using broadband 1.9–4.0 MHz transducers. Special care was taken to ensure that the LV was completely enclosed in the Doppler sector. The Doppler (velocity) and harmonic B-Mode (tissue-intensity) images were carefully recorded consecutively without displacing the probe, at respective frame rates of $29 \pm 6\ \text{s}^{-1}$ and $100 \pm 10\ \text{s}^{-1}$. At least five complete cardiac cycles were acquired in the color-Doppler mode. The electrocardiogram (EKG) signal, or the synthetic EKG *in vitro*, was recorded to allow matching the B-mode and Doppler data during the image postprocessing (see next subsection).

D. Echocardiographic Data Extraction

Echocardiographic raw data was extracted prior to scan conversion from the DICOM-III private tags (GE-proprietary format) by means of the HDF5 format using EchoPAC. These data include B-mode-derived ultrasound intensity, Doppler radial velocity, Doppler power, the position and size of the acquisition sector, the time values, and the EKG signal. The spatial resolution varied very little with the settings of the ultrasound machine (width and depth of the Doppler sector and Nyquist velocity). The radial step obtained *in vivo* was 0.540 ± 0.001 mm whereas the angular step was 0.019 ± 0.001 radians. Color–Doppler line sweep rate was 1400 Hz (1055–1610 Hz), for a mean frame rate of 32 Hz and sectors of 40–50 lines.

E. 2D Reconstruction of the Velocity Field

The consecutive steps of the numerical process are illustrated in Fig. 2. Low-power Doppler signals were zeroed out by thresholding their amplitude. The temporal resolution was increased by decoding Doppler velocities over several heart beats and retrospectively merging them into a synthetic cardiac cycle based on the offset of each frame to the EKG signal features. This type of retrospective segmentation is a typical method for increasing resolution and/or depth-of-view used in other cardiovascular imaging modalities such as 3D-echo, computed tomography, or MR. Notice that (1) is resolved time-independently in each given frame, and therefore, the accuracy of our method is not affected by the temporal resolution of the acquisition. However, the cycle merging algorithm was implemented with the double purpose of 1) providing a sensitive characterization of the fast changes of intraventricular flow dynamics, and 2) allowing second-step processing using time-resolved algorithms not presented here.

Doppler velocities of the merged cycle were dealiased and smoothed out using two consecutive filters: a 2D median filter that removed spurious values within a 3×3 neighborhood, and a 2D Gaussian averaging filter that eliminated small-scale velocity fluctuations and experimental noise. The respective standard deviations of the Gaussian kernel were set equal to 1.5 mm and 0.02 rad in order to conserve the large-scale flow structures of interest. The location of the ventricle walls was provided from the speckle-tracking algorithm of EchoPAC [26]. Boundary, grayscale and radial velocity data were finally resampled into a uniform time grid using a least-squares harmonic decomposition, choosing the number of harmonics which minimized Akaike's information criterion. The forcing term of the continuity equation, $\partial_\theta V_\theta$, and the weight function were calculated from (1) and (4) respectively. Finally, $\partial_\theta V_\theta$ was integrated within the region of interest using (3) and (5), and the boundary conditions in (6). 2D velocity maps and streamlines were overlaid on the B-mode images for visualization and clinical interpretation.

F. In Vitro Measurements

Experiments were performed using an atrio-ventricular dual activation pulse duplicator (IRPHE, Cardiovascular Biomechanics Team). This *in vitro* model consists of ventricular and atrial activation boxes, systemic and pulmonary circulation models, and a computerized driving interface [28], [29]. The left heart cavities are made up of silopren (General Electric Bayer Silicones) and are compliant and transparent. A liquid made of 40% glycerol and of 60% saline water was used as a blood substitute because its viscosity and density at room temperature are known to be similar to that of blood under high shear rates. The *in vitro* system was set to simulate three different hemodynamic conditions: heart rate (bpm)/stroke volume $(\mathrm{mL}) = 60/65$, 80/60 and 100/75. The velocity field within the ventricular cavity was measured using particle image velocimetry (PIV, [23]). The flow was highlighted with a double-pulse mini-YAG laser (120 mJ, $\mathrm{dt} = 1/15$ s between consecutive pulse pairs) synchronized to a 2 Mega pixel high-speed camera for two-frame PIV capture (TSI Inc., Shoreview, MN). The laser output was arranged as 1-mm-wide plane sheet that crossed the entire ventricular cavity. The laser plane cut the mitral and aortic valve planes as well as the apex to simulate an apical long-axis view. Neutrally-buoyant Nylon particles, with a mean diameter of 15–20 $\mu\mathrm{m}$ were used as markers. The delays between each pair of snapshots was $\Delta\mathrm{t} = 40 \pm 3$ ms. The image series were processed with a standard commercial software package (Insight3G, TSI Inc., Shoreview, MN) using interrogation windows of 64×64 pixels, providing a spatial resolution of 2×2 mm^2. Ensemble average velocity fields were obtained using 30 consecutive cycles. Echocardiographic acquisitions (see Section II-C) were performed immediately before the PIV measurements without interrupting the duplicator system.

G. In Vitro Validation of the Algorithm Used in the Reconstruction of the 2D Velocity Field

The *in vitro* PIV data at 60 bpm were used 1) to test the 2D-flow hypothesis separately from the echocardiographic acquisition and 2) to analyze the sensitivity of the method to the interrogation position of the Doppler sector. The radial $(V_{r\mathrm{PIV}})$ and azimuthal $(V_{\theta\mathrm{PIV}})$ components of the PIV velocity field were calculated in a polar coordinate system centered at an arbitrary apical point that represents the virtual location of the ultrasound transducer defined by the cartesian coordinates $(x_{\mathrm{VT}}, y_{\mathrm{VT}})$. To test the algorithm, we compared the reconstructed velocity field $(V_{\mathrm{rPIV}}, V_{\theta\mathrm{REC}})$ with the measured velocity field $(V_{r\mathrm{PIV}}, V_{\theta\mathrm{PIV}})$, where $V_{\theta\mathrm{REC}}$ was obtained from $V_{r\mathrm{PIV}}$ using (3), (5), and (6). These velocity fields should be identical provided that our numerical algorithm was exact and that the 2D-flow hypothesis was correct within the uncertainty margin introduced by the PIV measurement errors. The fact that both fields were discretized numerically on the same grid allowed their direct, pointwise comparison. The effect of the position and orientation of the ultrasound sector was tested by varying $(x_{\mathrm{VT}}, y_{\mathrm{VT}})$ and expressed by the angular offset (α). The pointwise error associated to the numerical reconstruction was defined as the absolute value of the difference between the PIV and the reconstructed velocity fields, $\varepsilon(x,y) = \|\vec{V}_{\mathrm{PIV}} - \vec{V}_{\mathrm{REC}}\|$. Finally, the overall relative error was defined as

$$E_{\mathrm{tot}} = \frac{\int_{LV} \varepsilon(x,y)dS}{\int_{LV} \|\overrightarrow{V}_{\mathrm{PIV}}\|dS} \tag{10}$$

where LV denotes the region of the acquisition plane inside the left ventricle and $\varepsilon(x,y)$ is the abovementioned pointwise error. Equivalent definitions were used to estimate absolute and relative error (E_θ) of the azimuthal component of the velocity fields (V_θ).

H. Reconstructed 2D Velocity Field: In Vitro PIV Versus Doppler Echocardiography

Because the 2D ultrasound scanning plane was slightly skewed (as deduced from the different PIV and Doppler sectors shown in Figs. 4 and 5), it was not possible to match completely the laser plane used in the PIV measurements; thus a pointwise comparison of the velocity fields obtained with the two methods was unfeasible. Instead, the integral properties of the flow structures were compared because they vary little with small changes in the observation plane. The position, radius and circulation of the main vortex that appears during diastole and isovolumic contraction were determined from both PIV and Doppler velocity data using [(7)–(9)], and their respective values were compared using absolute $(\mathrm{E_A})$ and relative $(\mathrm{E_{rel}})$ errors as well as the intraclass correlation coefficient $(\mathrm{R_{ic}})$.

I. Error Related to the Planar-Flow Assumption and Scan-Plane Misalignment: Phase-Contrast MR Studies

Phase-contrast MR sequences were obtained from two healthy volunteers, one patient with a chronic inferior myocardial infarction, and one patient with an idiopathic dilated cardiomyopathy. A 1.5-T unit (Philips Intera, software package release 9, The Netherlands) with a multielement phased array surface coil and retrospective EKG gating was used. Phase contrast velocity measurements were performed using a segmented fast gradient echo sequence (repetition time [ms/echo]/time [ms] 8.8/5.2; flip angle, 15°; section thickness, 8 mm; matrix, 304×300). Two direct orthogonal within-plane velocity measurements were obtained in scout-guided long-axis views, and used for reference (anteroposterior, with predefined upper velocity limit of 50 cm/s, and head–feet, with limit of 100 cm/s). In two of the volunteers, additional acquisitions were obtained at 8 mm parallel displacements of the scan plane.

Using this method, direct methods of the 2D velocity field were obtained. For *in vivo* validation of the planar flow hypothesis, the radial $(V_{r\mathrm{MR}})$ and azimuthal $(V_{\theta\mathrm{MR}})$ components of velocity were obtained from arbitrary reference points replicating the *in vitro* methodology described in Section II-G.

J. Clinical Application of the Color-Doppler Method

With the purpose of preliminary clinical testing, illustrative examples were obtained for two healthy volunteers, two patients with dilated cardiomyopathy, and two patients with severe cardiac hypertrophy due to advanced hypertensive cardiac disease. These disease conditions were selected because they represent extreme examples of abnormal LV geometries. Apical long axis

views were carefully aligned to depict the valvular landmarks described above and the color-Doppler sector was optimized to fit in the full LV cavity. During end-expiratory apnea, a run of 8–12 beats of color-Doppler images was acquired; then, without moving the probe, three beats of standard B-mode images were obtained during the same apnea. For all subjects, the images were obtained at color-Doppler acquisition frame-rates of 18 to 25 Hz, typically around 150–220 frames per acquisition. After cycle merging, all studies were re-interpolated to a single cycle of 200 frames. Typical processing time on a laptop computer equipped with a 2 GHz Centrino (Intel Corporation, Santa Clara, CA) processor and 2 GB RAM memory was 1–2 min to run the speckle-tracking software, followed by 3–5 min to obtain the full 2D+t velocity maps. This study has received approval from the Institutional Ethics Committee and informed consent was obtained from all subjects participating in the study.

III. Results

A. In Vitro Validation

2D Velocity Reconstruction Algorithm: Fig. 3 compares the *in vitro* flow field measured by PIV (V_{rPIV}, $V_{\theta\mathrm{PIV}}$, left column) with the field reconstructed using the algorithm (V_{rPIV}, $V_{\theta\mathrm{REC}}$, right column) for three instants of the cardiac cycle at 60 bpm. The results indicate that the reconstructed velocity field reproduced well the flow patterns during the filling of the *in vitro* model despite some slight, local discrepancies. This observation is also true for the position and size of the large recirculation region (Fig. 3, black circles) that formed in the core of the ventricle. The comparison of the PIV and reconstructed velocity fields deserved extra attention during systole because permeable boundary conditions were necessary on the outflow tract, which was perpendicular to the mitral inlet (Fig. 3, bottom). Notice however that the *in vivo* configuration was such that permeable boundary conditions were never necessary. The existence of permeable boundaries in the *in vitro* model complicated the reconstruction algorithm in two ways. First, the calculation of the azimuthal velocity at the left limit of the acquisition sector, $\theta^{-}(r)$, became nontrivial. Furthermore, flow velocities were typically one order of magnitude higher on the outflow tract than on the LV walls, and therefore the results were more sensitive to the boundary conditions imposed on this location. In spite of these added complexities, our reconstruction algorithm worked well also during ejection (Fig. 3, bottom).

The overall relative error associated to the reconstructed diastolic flow was nearly minimal when the Doppler sector axis was properly aligned with the apical long axis (Fig. 4(a) and (d), red squares and gray circles). In such condition, the error during diastole was $E_{\mathrm{tot}} \approx 0.15$, for the whole velocity vector [Fig. 4(d)] out of which the numerical procedures such as filtering and differentiation account for about one third. The error for the reconstructed azimuthal velocity component was around twice larger, $E_{\theta} \approx 0.3$ [Fig. 4(c)] but the large scale patterns of this velocity component were accurately captured [Fig. 4(b)]. In fact, a typical spatial distribution of the absolute error around this optimal alignment [Fig. 4(a)] shows an approximately random distribution associated to small scales. Consistent with this idea, we observed that error decreased when we increased

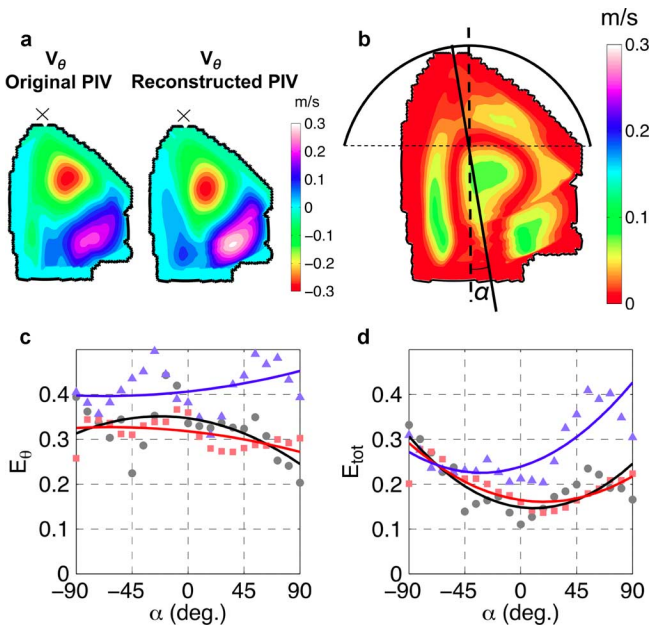

Fig. 4. Effect of the transducer position on the *in vitro* reconstructed velocity field. (a) Side-by-side comparison of the azimuthal component of the reconstructed velocity field (right) and the PIV measurements (left) during the late filling phase shown in Fig. 3 (central row). The data are represented in m/s using a color scale narrower than in Fig. 3 to enhance the differences between the two velocity fields. The radial components are equal (see Section II-G). (b) Absolute value of the difference between the azimuthal components of the reconstructed velocity field and the PIV measurements. The data come from the same instant of time during the late filling phase shown in Fig. 3 (central row). Velocity differences are represented in m/s using a color scale narrower than in Fig. 3 to enhance the differences between the two velocity fields. The black cross indicates the origin of the polar coordinate system. The semi-circle represents the varying positions of this origin considered in the elaboration of (c) and (d) and defined by the angle α. (c) Relative error of the azimuthal component of the reconstructed velocity field with respect to the PIV data as a function of the angleα. The data come from the same instants of time shown in Fig. 3 (60 bpm): •, rapid filling; ■, late filling; ▲, ejection. The solid curves are quadratic least square fits to the data. (d) Same as C for the total relative error of the whole velocity vector.

the width of the low-pass filter used in the calculation of $\vec{V}_{\mathrm{REC}}$ (see Section II-E).

Errors depended slightly on α around their minimum, indicating that the reconstruction method was little sensitive to misalignments of the ultrasound probe that might occur during clinical acquisitions. The overall error reached its maximal value ($E_{\mathrm{tot}} \approx 0.5$) when the virtual probe was oriented perpendicular to the apical axis ($\alpha = 90°$) so that only a small fraction of the velocity in the inflow or outflow jets was captured by the Doppler radial component. Under this configuration, the reconstruction algorithm strongly amplified small radial variations in V_{rPIV}, and became very sensitive to noise. During systole, the overall error did not fall below $E_{\mathrm{tot}} \approx 0.2$ due to the approximations related to permeable boundaries (Fig. 4(c), (d), blue triangles). This complication appeared exclusively *in vitro* as a consequence of the non-physiological location of the aortic valve in the silicone model. Note that such misalignment can be easily avoided *in vivo* by properly aligning the ultrasound probe with the LV apical axis such that α remains small. The maximum relative error during systole was achieved near $\alpha = 50°$, when the outflow jet was approximately normal to the virtual ultrasound beam. This angle is expected to be close to $\alpha = 90°$

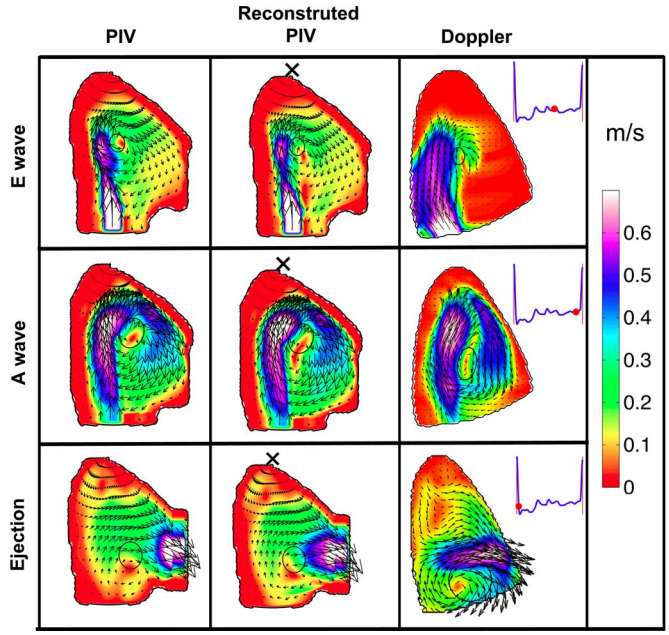

Fig. 5. Two-dimensional velocity field (m/s) in the vitro model at 100 bpm showing original PIV measurements (left column) versus 2D Doppler velocimetry (right column). The center column represents reconstructed measurements from the continuity equation as in Fig. 3. Black circles represent location and radius of the main swirling region, as in Fig. 3. Both color and arrow-length encode velocity magnitude.

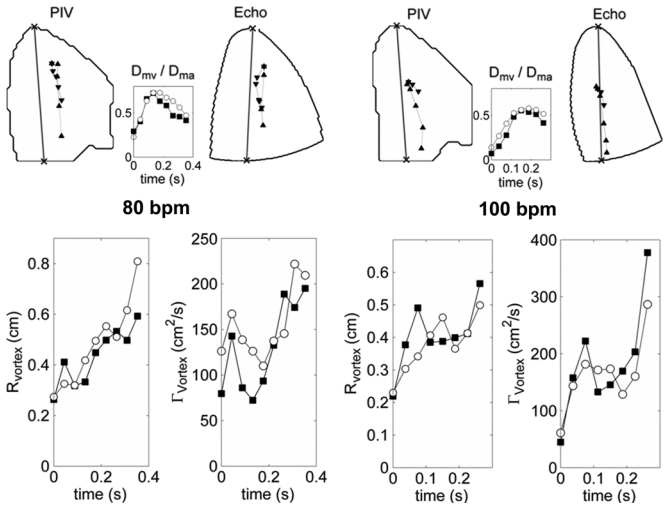

Fig. 6. PIV versus 2D Doppler velocimetry to account for trajectory (top panels) and properties (bottom panels) of the main swirling region that formed in the *in vitro* model during diastole and isovolumic contraction at 80 bpm (left) and 100 bpm (right). Top: ▲, the vortex is moving towards the apex (forward); ▼, the vortex is moving towards the base; ×—×, LV long axis. The insets in top panels show the time evolution of the distance from the vortex to the mitral valve $(\mathrm{D_{mv}})$ normalized to the length of the ventricular axis $(\mathrm{D_{ma}})$. ∘, PIV; ■, 2D Doppler. Bottom: time evolution of the radius $(\mathrm{R_{vor}})$ and circulation (Γ_{vor}) of the vortex, as measured by ∘, PIV and ■, 2D Doppler.

TABLE I

Heart rate		$\mathbf{R_{vortex}}$ **(t)**	$\mathbf{\Gamma_{vortex}}$ **(t)**	$\mathbf{D_{mv}/D_{ma}}$
80 bpm	E_A	-0.1±0.1 cm	-30 ± 40 cm^2/s	-0.044 ± 0.070
	E_{rel}	-10 ± 18 %	-23 ± 27 %	-6 ± 16%
	R_{ic}	0.73	0.52	0.87
100 bpm	E_A	0 ± 0.1 cm	20 ± 40 cm^2/s	-0.066 ± 0.039
	E_{rel}	6 ± 17 %	4 ± 25 %	-22 ± 18%
	R_{ic}	0.72	0.85	0.91

Differences between the properties of the LV vortex during diastole and isovolumic contraction obtained from PIV and the Doppler-based method *in vitro*. $\mathrm{R_{vortex}}$ is the vortex radius (see Eq. (9)), Γ_{vortex} is its circulation [see (7)] and $\mathrm{D_{mv}/D_{ma}}$ is the relative distance from the vortex to the mitral valve $(\mathrm{D_{mv}})$, normalized with the length of the ventricular long axis $(\mathrm{D_{ma}})$. $\mathrm{E_A}$ and $\mathrm{E_{rel}}$ are respectively the absolute and relative errors. These errors are expressed as $\mathrm{mean} \pm \mathrm{SD}$ (95% limits of agreement). $\mathrm{R_{ic}}$, is the intraclass correlation coefficient between the PIV and Doppler measurements.

in vivo since the angle between LV inflow and outflow tracts is approximately 10°–15° [17].

PIV vs. Color-Doppler Validation: Fig. 5 compares the *in vitro* flow field measured by PIV (left column) with that measured by color-Doppler for three instants of the cardiac cycle at 100 bpm (right column). While a perfect matching with the PIV and ultrasound planes was unfeasible (see Section II-H), a reasonable agreement was noticed between the two modalities except during ejection due to the presence of permeable boundaries (bottom row) related to the non-anatomic outflow tract in the *in vitro* model. The reconstructed PIV velocity field (center column) shows a similar agreement with that measured by echocardiography. A fair agreement was observed when comparing the radius and location of the main vortex (black circles), and even in the existence and location of a secondary vortex near the apex during ejection. This result also implies that the flow patterns varied little in the cross-plane direction, supporting the 2D hypothesis made in the reconstruction of the azimuthal velocity.

Fig. 6 shows the position, radius (R), and circulation (Γ) of the main vortex during diastole and isovolumic contraction as depicted by PIV and our Doppler-based method. A good agreement was observed between both techniques (Table I) despite the differences between the laser and insonation planes. At the onset of filling, both techniques identified the vortex ring associated to the starting mitral jet. The part of the vortex ring that was proximal to the wall decayed faster, while the distal part grew until it filled the whole ventricle at the end of diastole. During the rapid phase of ventricular filling (E wave), the vortex traveled towards the apex (forward), and then slowed down when it got closer to the apex (Fig. 6). When the second jet appeared (A wave), it turned around and traveled towards the base of the ventricle (backward). The radius of the vortex increased continuously from $\mathrm{R} \approx 0.2$ cm to $\mathrm{R} \approx 0.6$ cm, showing good agreement between PIV and Doppler (Fig. 6, bottom). The circulation inside the vortex, which defines its global strength, was also well reproduced by the Doppler-based method. Furthermore, it is interesting to remark that the method was able to capture the changes in the vortex dynamics of the *in vitro* model when the heart rate varied from 80 to 100 bpm. Indeed, the vortex got closer to the apex in its forward motion at 80 bpm (Fig. 6, left) than at 100 bpm (Fig. 6, right). Conversely, it moved closer to the base in its backward motion at the lower heart rate. The normalized distance from the vortex to the mitral valve was also measured accurately by Doppler (Fig. 6 top, insets).

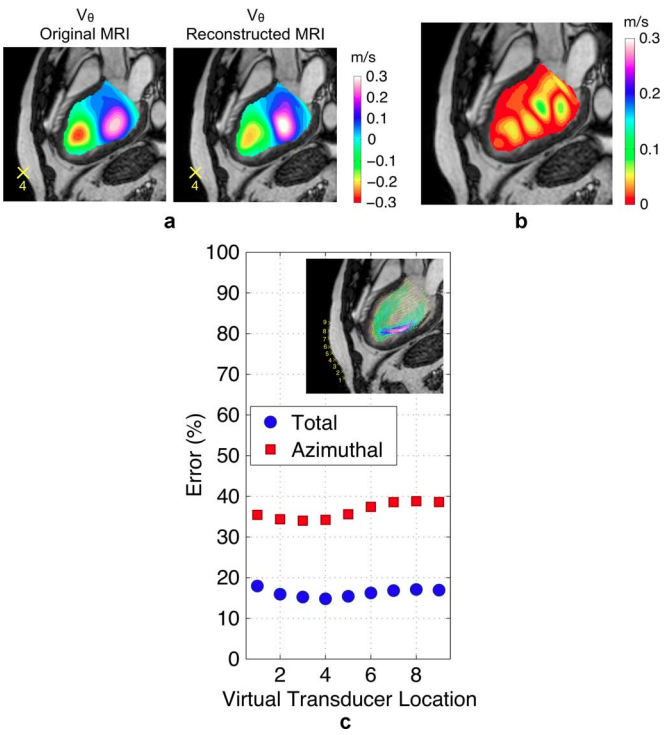

Fig. 7. Effect of the probe tilt on the *in vivo* reconstructed velocity field. The data come from an instant of time during the late filling phase in a patient with dilated cardiomyopathy. (a) Side-by-side comparison of the azimuthal component of the azimuthal velocity component obtained from MR, $\mathrm{V}_{\theta\mathrm{MR}}$, and the azimuthal velocity component reconstructed from the continuity equation, $\mathrm{V}_{\theta\mathrm{REC}}$. Both maps are obtained for the same location of the virtual probe, which is indicated by the yellow X. The data are represented in m/s. (b) Absolute value of the difference between the azimuthal components of the reconstructed velocity field and the MRI measurements. Velocity differences are represented in m/s. (c) Relative error of the total reconstructed velocity field (•), and of the azimuthal velocity component (■), with respect to the MR data [(10)] as a function of the position of the ultrasound virtual probe. The inset in the upper part of the panel shows an arrow plot of the blood velocity field obtained by phase contrast magnetic resonance imaging overlaid on an anatomical image. The yellow Xs mark the locations of the virtual probe considered for the calculation of the reconstruction error.

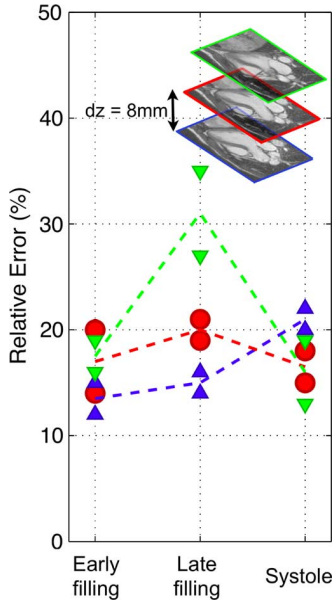

Fig. 8. Effect of the location of the insonated plane on the *in vivo* reconstructed velocity field. The plot shows the total relative error of the reconstructed velocity field with respect to the MR data [(10)] for three different long-axis planes separated a distance $\Delta z = 8$ mm. The inset in the upper part of the figure shows anatomical images of these three planes. The plane framed in red corresponds to a three-chamber apical long axis view. Data from three instants of the cardiac cycle of the two healthy volunteers. The dashed lines show the average error for each long-axis plane.

Finally, it should be taken into account that the PIV particle suspension employed in the silicon model produced relatively poor ultrasound backscatter. In fact, the Doppler signal received *in vitro* had typically half the power than *in vivo*. In this sense, the *in vitro* studies provided a conservative means of validation since higher measurement sensitivity is expected in the clinical studies.

B. In Vivo Hypothesis Validation

2D Velocity Reconstruction Algorithm: Fig. 7 compares the *in vivo* velocity field measured by phase contrast MR with the field reconstructed using the algorithm for an instant of late filling for a human volunteer. The intraventricular flow pattern in this case [see inset of Fig. 7(c)] consists of a large swirling region that occupies most of the ventricular cavity, in close agreement with the flow pattern previously described using MR [17], [19], [20]. Similar to the *in vitro* experiments, the overall relative error associated to the reconstructed diastolic flow was minimal and approximately equal to $E_{\mathrm{tot}} = 0.15\%$ when the Doppler sector axis was properly aligned with the apical long axis [Fig. 7(c)]. Also similar to the *in vitro* experiments, the error depended little on the location of the virtual transducer, indicating that the reconstruction method was robust with respect potential misalignments of the ultrasound probe. The results show that the azimuthal velocity field measured with MR ($\mathrm{V}_{\theta\mathrm{MR}}$, Fig. 7(a), left) around the optimal location of the virtual probe compares well with the field obtained by the reconstruction algorithm ($\mathrm{V}_{\theta\mathrm{REC}}$, Fig. 7(a), right), both qualitatively and quantitatively. Fig. 7(b) shows that the spatial structure of the error has smaller lengthscales than the azimuthal velocity.

Measurements of the overall relative error with respect to phase contrast MR data on different long-axis planes (Fig. 8) indicated that the reconstruction algorithm is fairly insensitive to the parallel displacement of the acquisition plane. The only exception to this behavior was observed during late diastole at the most lateral location considered, probably due to the smaller size of the imaged section (see inset of Fig. 8).

Also the phase contrast MR study (Fig. 9) showed that the overall relative error of the reconstruction algorithm was not affected by conditions such as dilated cardiomyopathy or chronic infarction. In all clinical cases studied and during all the time instants of the cardiac cycle considered, this error was bound between 15% and 20%.

C. Clinical Application of the Method

In normal subjects, the intraventricular flow pattern (see Fig. 10; Video #1 available at http://ieeexplore.ieee.org) closely matched features previously described using MR [17], [19], [20]. Strong filling jets emanating from the mitral valve were clearly visualized during rapid [E wave, Fig. 10(a)] and late (A wave) filling phases. These two filling jets feed a large diastolic vortex, which forms adjacent to the anterior mitral valve

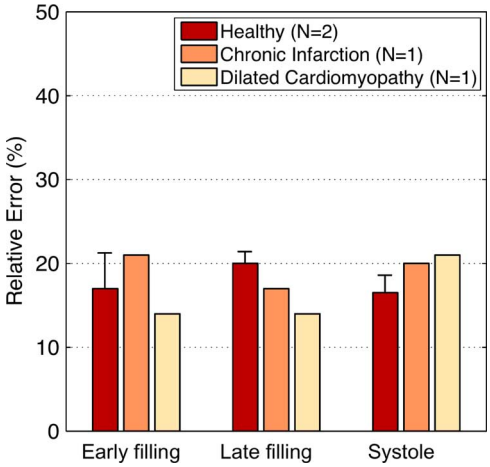

Fig. 9. Relative error of the reconstructed velocity field with respect to the MR data [(10) using $\varepsilon(x,y) = \|\vec{V}_{\mathrm{REC}} - \vec{V}_{\mathrm{MRI}}\|$] for different disease conditions. The data come from three instants of the cardiac cycle of two healthy volunteers, one patient with a chronic infarction and one patient with dilated cardiomyopathy.

leaflet at the onset of E wave deceleration. The diastolic vortex travels towards the inferior wall [Fig. 10(b)] while its size and circulation keep increasing, even when the inflow due atrial contraction decelerates. At the onset of the QRS complex of the electrocardiogram, the vortex is located close to the base and occupies almost the whole short diameter of the LV [Fig. 10(c)]. The circulation in the vortex is sustained during isovolumic contraction, while it redirects blood towards the outflow tract [Fig. 10(d)]. As the aortic valve opens, the circulation starts decreasing and, as a result, the vortex vanishes during ejection [Fig. 10(e)]. Finally, during isovolumic relaxation the blood velocity direction is reset towards the LV apex prior to opening of the mitral valve [Fig. 10(f)].

The method clearly identified different filling flow dynamics in abnormal heart geometries. In hypertrophic hearts, the early filling vortex was far more disorganized, including a recirculating cell in the apical region that does not contribute to efficient flow redirection towards the aortic valve during systole [Fig. 11(b)]. In dilated hearts early LV filling vorticity was also more disorganized with more frequent existence of counter-rotating vortex pairs that persisted throughout the whole filling phase (Fig. 11(c); Video 2 available at http://ieeexplore.ieee.org).

IV. Discussion

Cardiac pumping leads to the formation of large swirling regions in the heart cavities [17], [24]. The role of these flow structures as determinants and/or indicators of ventricular function is only now being considered due to difficulties in the measurement of whole intraventricular flow fields. This work introduces a novel, fully-noninvasive technique for imaging 2D blood velocities inside the LV based on Doppler-echocardiography. The velocity components normal to the ultrasound beams are estimated from the continuity equation, which is simplified based on the assumption that the large scales of the flow are approximately 2D in the plane of interest. Although further work is needed to validate the new modality *in vivo*, existing [25] as well as our own [30] (Figs. 7–9) MR measurements in humans support the 2D approximation. The adoption of a polar coordinate system greatly simplifies the computational routines, leading to an explicit formula for the reconstructed velocity component that can be expressed as a 1–D integral. This formula is overdetermined at all radial positions that have two LV wall velocity measurements, which allows us to cancel part of the error due to the planar flow assumption [(3)–(5)]. The reconstruction algorithm is applied to each single frame independently, which makes the estimated velocity insensitive to the time resolution of the acquisitions.

A. Comparison With Noninvasive Modalities

Presently, two methods are generally used to reconstruct a 2D flow field from ultrasound images: 1) cross-beam vector Doppler ultrasound using linear-array transducers [31]–[33] and 2) optical flow based on the normalized cross-correlation method carried out on B-mode frames obtained during contrast agent infusion (echo-PIV) [34]–[37]. The first method provides good results in vascular applications [38] but is not adapted to cardiac flow imaging since two measurements differing by a significant angle (ideally $> 10^{\circ}$) are needed [31]. More recently, the correlation analysis of synthetic aperture images has provided 2D velocity vectors in small bifurcating arteries with high resolution [39]–[41]. This method solves the signal-to-noise problems inherent to multiple-angle beaming but current hardware limitations restrict its field-of-view to about 3 cm, which is still unsuitable for intracardiac flows.

Echo-PIV requires continuous intravenous injection of contrast agent to acquire B-mode intensity images suited for the cross-correlation algorithm [36], [37], [42]. Due to the unstable nature of bubble aggregates in the LV as well as the effect of their interaction with ultrasound, a very complex fine-tuning of the contrast infusions before image acquisition is needed [43]. Besides, the size of the interrogation window and the spatiotemporal resolution requirements currently restrict echo-PIV to small acquisition sectors. Spatial resolution has also recently shown to be lower than expected [42]. Nevertheless, this technique has proven to be useful to derive important physiological information from the visualization of 2D flow mapping in the experimental setting [37].

Phase-contrast cardiac MR has been useful to illustrate the spatial complexity of the flow patterns in the LV [17], [19], [20], [44]. Despite the technique has been available for more than 10 years, a comprehensive clinical characterization of intracardiac flow dynamics in different disease states has never been performed probably due to the lack of availability and complexity of the technique.

Clinical acceptance of new imaging tools relies on criteria that do not always take priority in the development of engineering concepts: they need to be relatively uncomplicated, fast (no lengthy offline analysis) and economically affordable [45]. The new modality proposed in this work provides investigators with a fast, portable, workable and totally noninvasive process for displaying a 2D vectorial flow-field of the LV. It is based on echocardiographic acquisitions that take less than 1 min, and the ensuing offline processing is completed in approximately 5 min using off-the-shelf computing equipment (see Section II-J).

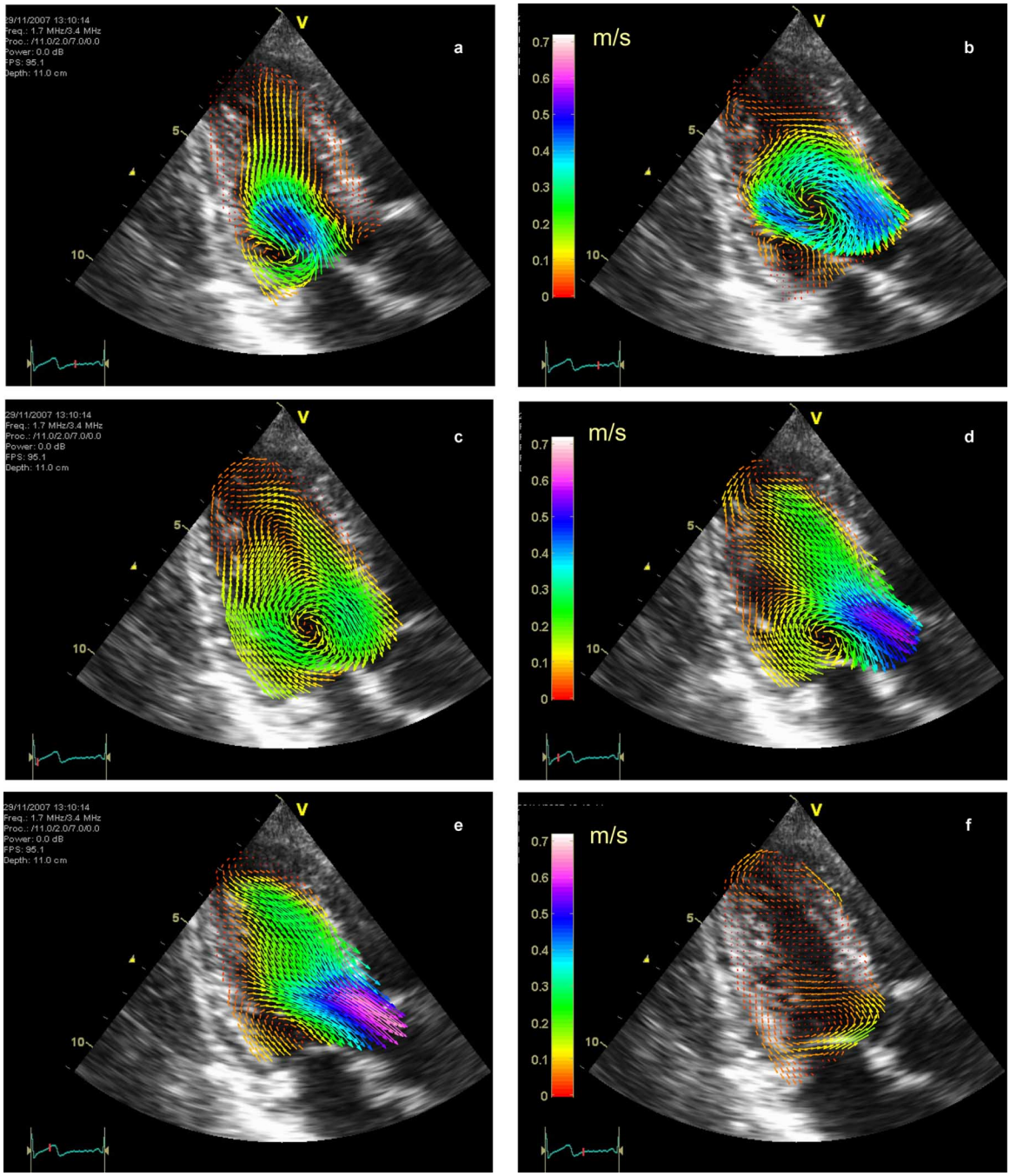

Fig. 10. Blood velocity mapping in a normal LV overlaid on a sequence of anatomical B-mode apical long-axis images during (a) rapid filling, (b) late filling, (c) isovolumic contraction, (d) ejection onset, (e) ejection, (f) isovolumic relaxation. The vectors indicate the direction and magnitude of the velocity as coded in the color bars (m/s). The bottom left corner shows the electrocardiogram. Both color and arrow-length encode velocity magnitude.

Special efforts have been taken to work with the full bit-depth raw-velocity data as measured by the Doppler autocorrelator, and to develop a custom algorithm to increase the temporal resolution of color-Doppler. We have previously demonstrated these are necessary requirements to allow further postprocessing in order to exploit the full physiological information embedded in the velocity data [46]. We have shown that the new modality is relatively insensitive to small misalignments of the ultrasound probe that might occur during clinical acquisitions [see Fig. 4(c) and (d) and Fig. 7(c)], which together with the fact that it uses conventional echocardiographic views, imposes little ultrasonographer training. Finally, this technique is the only available method for patients with implanted pacemakers and cardiac resynchronization devices who cannot undergo MR safely.

B. *Limitations of the Study*

Although it is partially relaxed by the existence of two wall LV wall velocity measurements at each radial position, the assumption of 2D-flow intraventricular is a hard constraint for the method that deserves an important validation effort. Both our *in vitro* comparison against PIV and *in vivo* comparison against

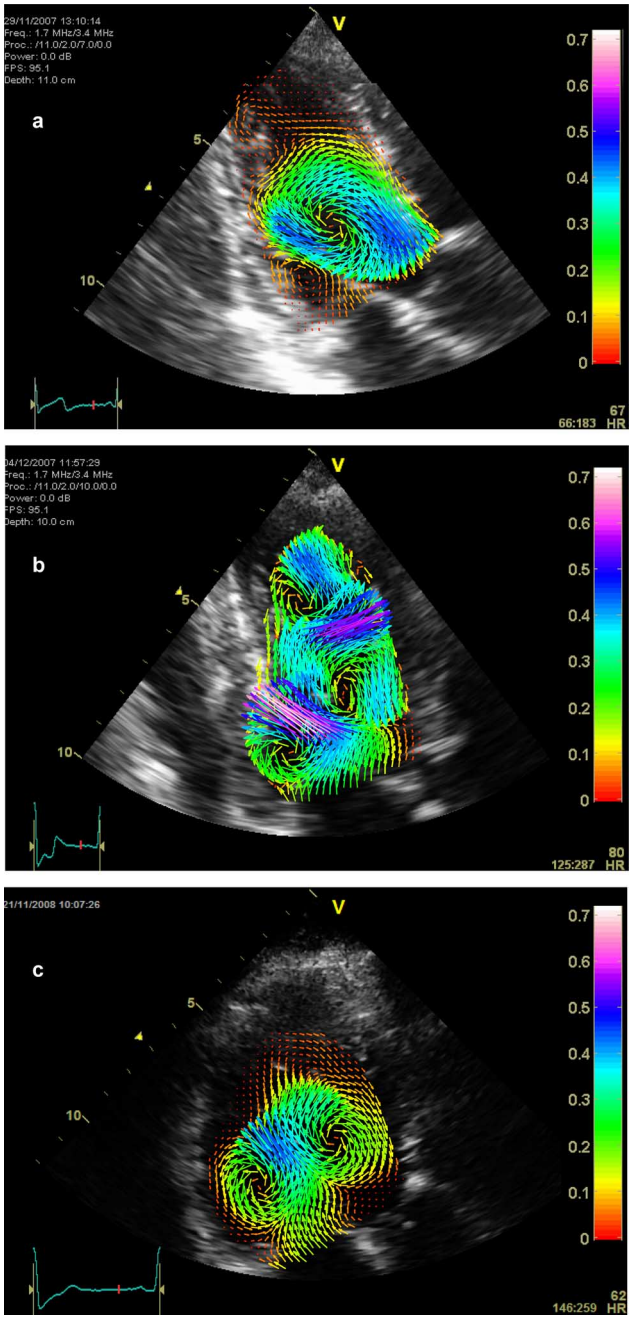

Fig. 11. Blood velocity mapping in volunteers overlaid on anatomical B-mode apical long-axis images. (a) normal, (b) hypertrophied, and (c) dilated ventricle. The color shades indicate the magnitude of the velocity as coded by the color bars and the black lines show the streamlines, which are parallel to the velocity vector at each point. The arrow heads on the streamlines indicate the direction of the flow. Both color and distance between neighboring streamlines encode velocity magnitude.

MR suggested that the 2D-flow hypothesis is acceptable in the apical long-axis view. In particular, the spatial distribution of the estimated reconstruction error had a small-scale appearance, suggesting that no systematic deviations were present in the method. The validation results *in vitro* are encouraging given that the Doppler signal was roughly half the amplitude *in vitro* than *in vivo*. Furthermore, it was not possible to match completely the PIV and ultrasound scanning planes during the acquisition. Even so, we obtained reasonably accurate validation of the vortex features, suggesting that the starting assumption stands fairly well in normal geometry ventricles. The results of the MR study also confirmed that the planar flow assumption is assumable *in vivo* both in normal as well as in clearly abnormal LV geometries.

A number of well established three-dimensional cardiovascular indices are routinely applied on the basis of practical simplifications to guide patient care in everyday clinical practice. Measuring physiological indices using simplifications by means of 2D or even 1D assumptions is very frequent in cardiovascular medicine (LV volumes, myocardial strain, or color-flow propagation velocity, amongst others). Long-term studies have demonstrated that the clinical efficacy of these simplified methods in terms of clinical decision making, and mortality and morbidity avoided, definitely outweighs their technical inaccuracy [1]. Similarly, we believe that the error related to the method presented in our study allows measuring major intraventricular flow features to a degree that should be suitable for a clinical qualitative analysis such as the one presented here. Nevertheless, only a head-to-head comprehensive validation study against phase-contrast MR, and including several patient groups may clarify the final efficacy of this new technique in the armamentarium of noninvasive clinical cardiovascular imaging. Although our pilot clinical studies suggest that the proposed modality is fairly reproducible, a formal assessment of reproducibility would be desirable.

Frame interleaving for increasing temporal resolution is unsuitable in the presence of irregular heart rhythms, and for the present algorithm, heart cycles showing $>10\%$ variation were automatically discarded. Despite spatial resolution may be also slightly penalized, retrospective frame interleaving has proved to be crucial in other cardiac imaging modalities such as full-volume 3D echocardiography, cine-MR, and computed tomography angiography.

C. Future Developments and Potential Clinical Applications

Two-dimensional echocardiographic intraventricular flow mapping is an inexpensive, noninvasive method to assess global LV function directly from 2D+t blood velocity data. We have already discussed how this method can be used to track and characterize intraventricular flow dynamics. Apart from this, the 2D+t velocity reconstruction technique developed in this work can be used to improve the accuracy of existing echocardiographic modalities that have relied on the assumption of 1D flow. One of them is the propagation velocity of the intraventricular filling wave, which is measured simply as slope of the color-Doppler M-mode recording and has been shown to be a useful prognostic parameter in patients after an acute myocardial infarction [47]. Another modality based on the 1D-flow hypothesis is the measurement of intracardiac pressure gradients along the inflow and outflow jets by applying the 1D Euler equation to color M-mode Doppler data [3], [48], [49]. Using this technique, new insight into important aspects of cardiovascular function have been described in the clinical setting [4], [6]. It is recognized that access to the full 2D flow velocity map would not only increase the accuracy of the above-mentioned techniques, but also expand their applicability to a

broader number of patients, disease conditions, and intracardiac locations [50]. The 2D Euler equations could now be applied to the 2D intraventricular flow to depict a full mapping of the relative pressure within the LV. Finally, it should be pointed out that, although this work has focused on the application of 2D+t velocity reconstruction to conventional echocardiographic acquisitions, this technique may be combined with other ultrasound modalities such as multiple-angle beaming [38] and synthetic aperture imaging [39], [40] to potentially improve their accuracy.

V. Conclusion

In the present study we propose a novel noninvasive modality that allows investigators to display the time evolution of 2D flow fields in the apical long axis view of the LV using color-Doppler echocardiography. Such flow fields are overlaid on grayscale anatomical images, allowing both visual and quantitative characterization of intraventricular flow features at a high temporal resolution. Compared with most existing noninvasive modalities, the method is fast, clinically compliant, and requires little training. Altghough a comprehensive validation study is required, this new modality offers the possibility of studying a number of unexplored aspects of intraventricular flow dynamics in the clinical setting by high-throughput processing conventional color-Doppler images.

Acknowledgment

The *in vitro* model was developed in collaboration with Dr. P. Pibarot. Assistance with the PIV system from J. Stefanini is also appreciated. Finally, it is a pleasure to acknowledge fruitful discussions with Dr. M. Alhama and professor J. C. Lasheras.

References

[1] M. D. Cheitlin *et al.*, "ACC/AHA/ASE 2003 guideline update for the clinical application of echocardiography—Summary article: A report of the American College of Cardiology/American Heart Association Task Force on Practice Guidelines (ACC/AHA/ASE committee to update the 1997 guidelines for the clinical application of echocardiography)," *J. Am. Coll. Cardiol.*, vol. 42, pp. 954–970, 2003.

[2] J. R. Thornbury, "Eugene W. Caldwell lecture. Clinical efficacy of diagnostic imaging: Love it or leave it," *Am. J. Roentgenol.*, vol. 162, pp. 1–8, 1994.

[3] R. Yotti *et al.*, "Noninvasive assessment of ejection intraventricular pressure gradients," *J. Am. Coll. Cardiol.*, vol. 43, pp. 1654–1662, 2004.

[4] R. Yotti *et al.*, "Doppler-derived ejection intraventricular pressure gradients provide a reliable assessment of left ventricular systolic chamber function," *Circulation*, vol. 112, pp. 1771–1779, 2005.

[5] J. D. Thomas and Z. B. Popovic, "Assessment of left ventricular function by cardiac ultrasound," *J. Am. Coll. Cardiol.*, vol. 48, pp. 2012–2025, 2006.

[6] C. Cortina *et al.*, "Noninvasive assessment of the right ventricular filling pressure gradient," *Circulation*, vol. 116, pp. 1015–1023, 2007.

[7] K. Namekawa *et al.*, "Realtime bloodflow imaging system utilizing auto-correlation techniques," *Ultrasound Med. Biol.*, pp. 203–208, 1983.

[8] H. Watanabe *et al.*, "Multiphysics simulation of left ventricular filling dynamics using fluid-structure interaction finite element method," *Biophys J*, vol. 87, pp. 2074–2085, 2004.

[9] Y. Cheng *et al.*, "Fluid-structure coupled CFD simulation of the left ventricular flow during filling phase," *Ann. Biomed. Eng.*, vol. 33, pp. 567–576, 2005.

[10] G. Pedrizzetti and F. Domenichini, "Nature optimizes the swirling flow in the human left ventricle," *Phys. Rev. Lett.*, vol. 95, p. 108101, 2005.

[11] H. Oertel *et al., Modelling the Human Cardiac Fluid Mechanics*. Karlsruhe: Univ. Karlsruhe, 2006.

[12] F. Liang *et al.*, "A multi-scale computational method applied to the quantitative evaluation of the left ventricular function," *Comput. Biol. Med.*, vol. 37, pp. 700–715, 2007.

[13] J. Cooke *et al.*, "Characterizing vortex ring behavior during ventricular filling with Doppler echocardiography: An in vitro study," *Ann. Biomed. Eng.*, vol. 32, pp. 245–256, 2004.

[14] O. Pierrakos and P. P. Vlachos, "The effect of vortex formation on left ventricular filling and mitral valve efficiency," *J. Biomech. Eng.*, vol. 128, pp. 527–539, 2006.

[15] F. Domenichini *et al.*, "Combined experimental and numerical analysis of the flow structure into the left ventricle," *J. Biomechan.*, vol. 40, pp. 1988–1994, 2007.

[16] A. Kheradvar *et al.*, "Correlation between vortex ring formation and mitral annulus dynamics during ventricular rapid filling," *ASAIO J.*, vol. 53, pp. 8–16, 2007.

[17] P. J. Kilner *et al.*, "Asymmetric redirection of flow through the heart," *Nature*, vol. 404, pp. 759–761, 2000.

[18] W. C. Little, "Diastolic dysfunction beyond distensibility: Adverse effects of ventricular dilatation," *Circulation*, vol. 112, pp. 2888–2890, 2005.

[19] L. Wigstrom *et al.*, "Particle trace visualization of intracardiac flow using time-resolved 3D phase contrast MRI," *Magn. Reson. Med.*, vol. 41, pp. 793–799, 1999.

[20] A. F. Bolger *et al.*, "Transit of blood flow through the human left ventricle mapped by cardiovascular magnetic resonance," *J. Cardiovasc. Magn. Reson.*, vol. 9, pp. 741–747, 2007.

[21] P. J. Kilner *et al.*, "Flow measurement by magnetic resonance: A unique asset worth optimising," *J. Cardiovasc. Magn. Reson.*, vol. 9, pp. 723–728, 2007.

[22] J. Lotz *et al.*, "Cardiovascular flow measurement with phase-contrast MR imaging: Basic facts and implementation," *Radiographics*, vol. 22, pp. 651–71, May–Jun. 2002.

[23] C. E. Willert and M. Gharib, "Digital particle image velocimetry," *Experiments in Fluids*, vol. 10, pp. 181–193, 1991.

[24] O. Rodevand *et al.*, "Diastolic flow pattern in the normal left ventricle," *J. Am. Soc. Echocardiogr.*, vol. 12, pp. 500–507, 1999.

[25] R. B. Thompson and E. R. McVeigh, "Fast measurement of intracardiac pressure differences with 2D breath-hold phase-contrast MRI," *Magn. Reson. Med.*, vol. 49, pp. 1056–1066, 2003.

[26] Y. Notomi *et al.*, "Measurement of ventricular torsion by two-dimensional ultrasound speckle tracking imaging," *J. Am. Coll. Cardiol.*, vol. 45, pp. 2034–2041, 2005.

[27] J. C. R. Hunt *et al., Eddies, Streams, and Convergence Zones in Turbulent Flows*. Stanford, CA: Center Turbulence Res., pp. 193–208.

[28] F. Mouret *et al.*, "Mitral prosthesis opening and flow dynamics in a model of left ventricle: An in vitro study on a monoleaflet mechanical valve," *Cardiovasc. Eng.*, vol. 5, pp. 13–20, 2005.

[29] D. Tanne *et al.*, "Assessment of left heart and pulmonary circulation flow dynamics by a new pulsed mock circulatory system," *Experiments Fluids*, vol. 48, pp. 837–850, 2009.

[30] J. C. Del Alamo *et al.*, "Recent advances in the application of computational mechanics to the diagnosis and treatment of cardiovascular disease," *Rev. Esp. Cardiol.*, vol. 62, pp. 781–805, 2009.

[31] B. Dunmire *et al.*, "Cross-beam vector Doppler ultrasound for angle-independent velocity measurements," *Ultrasound Med. Biol.*, vol. 26, pp. 1213–1235, 2000.

[32] L. Capineri *et al.*, "A Doppler system for dynamic vector velocity maps," *Ultrasound Med. Biol.*, vol. 28, pp. 237–248, 2002.

[33] O. D. Kripfgans *et al.*, "Vector Doppler imaging of a spinning disc ultrasound Doppler phantom," *Ultrasound Med. Biol.*, vol. 32, pp. 1037–1046, 2006.

[34] L. N. Bohs *et al.*, "Speckle tracking for multi-dimensional flow estimation," *Ultrasonics*, vol. 38, pp. 369–375, 2000.

[35] L. C. Lin *et al.*, "Power Doppler-derived speckle tracking image of intraventricular flow in patients with anterior myocardial infarction: Correlation with left ventricular thrombosis," *Ultrasound Med. Biol.*, vol. 26, pp. 341–346, 2000.

[36] H. B. Kim *et al.*, "Echo PIV for flow field measurements in vivo," *Biomed. Sci. Instrum.*, vol. 40, pp. 357–363, 2004.

[37] P. P. Sengupta *et al.*, "Left ventricular isovolumic flow sequence during sinus and paced rhythms," *J. Am. Coll. Cardiol.*, vol. 49, pp. 899–908, 2007.

[38] M. Arigovindan *et al.*, "Full motion and flow field recovery from echo Doppler data," *IEEE Trans. Med. Imag.*, vol. 26, no. 1, pp. 31–45, Jan. 2007.

[39] J. A. Jensen *et al.*, "Synthetic aperture ultrasound imaging," *Ultrasonics*, vol. 44, pp. e5–e15, 2006.
[40] J. A. Jensen and N. Oddershede, "Estimation of velocity vectors in synthetic aperture ultrasound imaging," *IEEE Trans. Med. Imag.*, vol. 25, no. 12, pp. 1637–1644, Dec. 2006.
[41] J. Udesen *et al.*, "Examples of in vivo blood vector velocity estimation," *Ultrasound Med. Biol.*, vol. 33, pp. 541–548, 2007.
[42] A. Kheradvar *et al.*, "Echocardiographic particle image velocimetry: A novel technique for quantification of left ventricular blood vorticity pattern," *J. Am. Soc. Echocardiogr.*, vol. 23, pp. 86–94, 2010.
[43] P. Vennemann *et al.*, "In vivo whole-field blood velocity measurement techniques," *Experiments Fluids*, vol. 42, pp. 495–511, 2007.
[44] W. Y. Kim *et al.*, "Left ventricular blood flow patterns in normal subjects: A quantitative analysis by three-dimensional magnetic resonance velocity mapping," *J. Am. Coll. Cardiol.*, vol. 26, pp. 224–238, 1995.
[45] B. B. Lieber *et al.*, "Correlation of hemodynamic events with clinical and pathological observations," *Ann. Biomed. Eng.*, vol. 33, pp. 1695–1703, 2005.
[46] J. L. Rojo-Alvarez *et al.*, "Impact of image spatial, temporal, and velocity resolutions on cardiovascular indices derived from color-Doppler echocardiography," *Med. Image Anal.*, vol. 11, pp. 513–525, 2007.
[47] J. E. Moller *et al.*, "Pseudonormal and restrictive filling patterns predict left ventricular dilation and cardiac death after a first myocardial infarction: A serial color M-mode Doppler echocardiographic study," *J. Am. Coll. Cardiol*, vol. 36, pp. 1841–1846, 2000.
[48] N. L. Greenberg *et al.*, "Estimation of diastolic intraventricular pressure gradients from color Doppler M-mode spatiotemporal velocities: Analytical Euler equation solution," *Comput. Cardiol.*, pp. 465–468, 1994.
[49] J. Bermejo *et al.*, "Spatio-temporal mapping of intracardiac pressure gradients. A solution to Euler's equation from digital postprocessing of color Doppler M-mode echocardiograms," *Ultrasound Med. Biol.*, vol. 27, pp. 621–630, 2001.
[50] J. D. Thomas and Z. B. Popovic, "Intraventricular pressure differences: A new window into cardiac function," *Circulation*, vol. 112, pp. 1684–1686, 2005.